LAWRENCE
LIVERMORE
NATIONAL
LABORATORY

LLNL-JRNL-818038

Multichannel Deconvolution of Vibrational Signals: A State-Space Inverse Filtering Approach

J. V. Candy, K. A. Fisher, B. A. Markowicz, D. J. Paulsen

January 4, 2021

Journal of the Acoustical Society of America

Multichannel Deconvolution of Vibrational Signals: A State-Space Inverse Filtering Approach

J. V. Candy, K. A. Fisher, B. A. Markowicz, D. J. Paulsen

Lawrence Livermore National Laboratory

P.O. Box 808, L-151

Livermore, CA 94551

Phone: 925-422-8675

Deconvolution of noisy measurements, especially when they are multichannel, has always been a challenging problem. The development of processing techniques range from simple Fourier methods to more sophisticated model-based parametric methodologies based on the underlying acoustics of the problem at hand. Methods relying on multichannel mean-squared error processors (Wiener filters) have evolved over long periods from the seminal efforts in seismic processing. However, when more is known about the acoustics, then model-based state-space techniques incorporating the underlying process physics can improve the processing significantly. The problem of interest is the vibrational response of a tightly-coupled acoustic test object excited by an out-of-the-ordinary, transient, potentially impairing its operational performance. Employing a multiple input/multiple output structural model of the test object under investigation enables the development of an inverse filter by applying subspace identification techniques during initial calibration measurements. Feasibility applications based on a mass transport experiment and test object calibration test demonstrate the ability of the processor to extract the excitation successfully even in the case of random excitations.

PACS numbers: 43.60.Uv, 43.60.Gk, 43.60.Cg, 43.30.Zk

I INTRODUCTION

When transporting delicate acoustical objects of interest, out-of-the ordinary, transient events can occur affecting overall system performance creating great concern. Events that can occur are essentially pulse-like, transient signals of short duration that evolve from various phenomena. Here the event can be created by either dropping of a test object during shipping/packing subjecting it to a compact high-energy blow or the object being struck unintentionally during transit resulting in potential damage or even just the typical random vibrations evolving from roadway, rail or flight turbulence. The intensity and location of the strike can cause an inoperability condition that is totally unacceptable. Therefore, it is essential to detect, classify and localize damage of any test object subjected to a shock event. This effort is aimed at evaluating the vibrational response of acoustical test objects that are subjected to "transport" shocks and roadway vibrations during shipping and handling as well as any test object subjected to random vibrations—another common event during transport. Any potential damage that could be inflicted during transportation must not only be detected, but also evaluated to determine the operational readiness of the test object before and after transport.[1−6]

The estimation of excitation signals from noisy data is termed the deconvolution problem in the signal processing literature. The *deconvolution problem* is based on recovering the input excitation signal(s) from a system characterized by its impulse response sequence.[7−11] Using this model of the system, an "inverse" representation or filter is developed to remove the system from the measured data and recover the input.[1,12,13] Deconvolution has long been a problem of great interest especially in the seismic community where the source location and extraction problem is one of great interest in localizing earthquakes and other phenomena.[1,2] Explosives in ocean acoustics have also been acoustic sources, desirable or undesirable, for both exploration and mapping leading to a transient deconvolution problem of high interest.[3,4] Deconvolution problems in nondestructive evaluation (*NDE*), room acoustics and structural vibration problems abound.[8,14,15]

Multichannel processing methods evolve from a variety of acoustic applications in spectral estimation, ocean acoustics, structural acoustics and more.[16−19] Model-based methods show improved performance with multiple input/multiple output (*MIMO*) constructs incorporating embedded models such as finite impulse response, autoregressive moving average and state-space models that are prevalent in spectral estimation and structural vibration analysis.[15−17] In this paper, the state-space approach is employed for a number of reasons, not just because the systems under investigation are primarily structural and can easily be captured within this framework, but also because they can be physically represented by a multichannel, linear time-invariant (*LTI*), mass-damper-spring (*MCK*) vibrating structure along with the added advantage of existing numerically stable subspace estimation techniques.[15,19−21]

The evolution of multichannel techniques for deconvolution has progressed significantly since the pioneering work of Robinson in the development of a recursive, mean-squared error (Wiener) method based on an *FIR*-representation and efficient Levinson methodology.[2,22,23] Following this work other methods evolved especially in spectral estimation applied to acoustic problems (e.g. ocean acoustics, sonar, seismology, *NDE*) as well as state-space techniques.[24−26] The state-space approach coupled to the well-known Kalman filter processor has evolved from seismic applications incorporating a well-defined geophysical model.[25] Since deconvolution is essentially an ill-conditioned *inverse problem*, an alternative methodology has evolved in ocean acoustics termed matched-field processing (*MFP*) primarily aimed at target localization and tracking.[26] In this approach measured multichannel field data are compared to that predicted by a propagation model, maxima or minima are then calculated based on various criteria to locate the target(s) position.[26] Another recent model-based approach incorporating a transient model has evolved using a forward modeling technique coupled to a Kalman filter, similar to the matched-field approach.[26,27] In this method, a Kalman filter with its embedded system model identified from experimental data, is employed in an iterative scheme to extract a parameterized transient.[26,27]

There are two candidate approaches that can be used to mitigate this multichannel problem. The first is the well-known Wiener least-squares solution employing the nonparametric multichannel Levinson algorithm.[2,22,24] The second approach, that is pursued in this paper, incorporates a state-space model that can be used to develop an inverse filter directly from input/output data. This approach incorporates any existing modal coupling that exists in the underlying structure being identified. That is, the state-space approach is to estimate the response of an underlying linear time-invariant, multichannel structural system using a black-box state-space model. This model captures the underlying structural dynamics of critical components enabling a viable vibration analysis to ensure that even weakly coupled modal signals buried in the noise are represented. Thus the primary contribution of this paper is to develop an inverse system design technique from calibration measurements employing subspace identification methodology and applying the resulting design as a filter to solve the multichannel deconvolution problem.[20,28–30]

The development of the underlying structural system and its incorporation into the state-space framework is developed in Sec. II. Next the deconvolution problem is defined in terms of multichannel input/state/output system descriptions and their equivalence. This is followed by the description of stochastic representations including the Gauss-Markov and innovations models leading to the state-space description of the inverse (shaping) filter along with its design—the primary mechanism employed in this effort. The design and application of the inverse filter for multichannel deconvolution is discussed in Sec. III after briefly describing a set of various transient shock signals that typically occur during transit. Two applications are discussed in detail. First a noisy mass-simulation transportation data experiment obtained by transporting a large-mass concrete block using a tractor/tailer vehicle on typical roadways followed by the vibrational response experiment of a test object excited by random excitations completing the study. The results of this work are summarized in the final section.

II. BACKGROUND

In this section, multiple channel structural vibration models are briefly developed leading to a set of deterministic as well as stochastic state-space models that are employed throughout to solve the deconvolution problem. The multichannel aspects of this problem are defined in terms of the state-space realization enabling it to uniquely characterize the problem and proceed with its solution.

A. Vibrational State-Space Model

Mechanical systems are important in many applications, especially when considering vibrational responses of critical components such as turbine-generator pairs in nuclear systems on ships or even in power generating plants at home as well as aircraft structures that transport people throughout the world. Next we briefly present the generic multivariable mechanical system representation that will be employed in examples and case studies to follow.

A multichannel, linear, time-invariant mechanical system can be characterized by

$$M\ddot{\mathbf{d}}(\tau) + C_d\dot{\mathbf{d}}(\tau) + K\mathbf{d}(\tau) = B_p\mathbf{p}(\tau) \tag{1}$$

where $\mathbf{d}$ is the $N_d \times 1$ displacement vector, $\mathbf{p}$ is the $N_p \times 1$ excitation force, and M, C_d, K, are the $N_d \times N_d$ lumped mass, damping, and spring constant matrices characterizing the vibrational process model, respectively and B_p is the input weighting matrix.

Define the $2N_d$-state vector as $\mathbf{x}(\tau) := \left[\ \mathbf{d}(\tau)\ \mid\ \dot{\mathbf{d}}(\tau)\ \right]^T$, then the continuous-time (τ) state-space representation of this process can be expressed as

$$\dot{\mathbf{x}}(\tau) \;=\; \underbrace{\left[\begin{array}{c|c} 0 & I \\ --- & --- \\ -M^{-1}K & -M^{-1}C_d \end{array}\right]}_{A_c}\mathbf{x}(\tau) + \underbrace{\left[\begin{array}{c} 0 \\ --- \\ M^{-1}B_p \end{array}\right]}_{B_c}\mathbf{p}(t) \tag{2}$$

or more compactly

$$\dot{\mathbf{x}}(\tau) = A_c\mathbf{x}(\tau) + B_c\mathbf{p}(t) \tag{3}$$

for A_c and B_c the appropriately dimensioned continuous-time (subscript c) system and input transmission matrices.

The corresponding measurement or output vector relation can be obtained from

$$\mathbf{y}(\tau) = \mathbf{C_a}\ddot{\mathbf{d}}(\tau) + \mathbf{C_v}\dot{\mathbf{d}}(\tau) + \mathbf{C_d}\mathbf{d}(\tau) \tag{4}$$

where the constant matrices: $\mathbf{C_a}, \mathbf{C_v}, \mathbf{C_d}$ are the respective acceleration, velocity and displacement weighting matrices of appropriate dimension.

Solving for the acceleration in Eq. 1 and substituting for this term in Eq. 4, gives

$$\mathbf{y}(\tau) = \underbrace{\left[C_d - \mathbf{C_a} M^{-1} K \;\;|\;\; \mathbf{C_v} - \mathbf{C_a} M^{-1} \mathbf{C_d}\right]}_{C_c} \begin{bmatrix} \mathbf{d}(\tau) \\ --- \\ \dot{\mathbf{d}}(\tau) \end{bmatrix} + \underbrace{\mathbf{C_a} M^{-1} B_p}_{D_c} \mathbf{p}(\tau) \tag{5}$$

to yield the vibrational measurement in terms of the state-space model as:

$$\mathbf{y}(\tau) = C_c \mathbf{x}(\tau) + D_c \mathbf{u}(\tau) \tag{6}$$

where the continuous-time output or measurement vector is $\mathbf{y} \in \mathcal{R}^{N_y \times 1}$ completing the deterministic multiple input/multiple output (*MIMO*) vibrational state model.

Corresponding to this continuous-time representation is its discrete-time counterpart consisting of similar state/measurement relations:

$$\begin{aligned} \mathbf{x}(t+1) &= A\mathbf{x}(t) + B\mathbf{u}(t) && \text{[State]} \\ \mathbf{y}(t) &= C\mathbf{x}(t) + D\mathbf{u}(t) && \text{[Measurment]} \end{aligned} \tag{7}$$

with appropriately dimensioned matrices defined by the model set $\Sigma_{ABCD} := \left\{A, B, C, D\right\}$

The discrete *transfer function* matrix is defined in terms of the $\mathcal{Z}$-transform

$$\mathcal{H}(z) = C(zI - A)^{-1}B + D \tag{8}$$

with the *impulse response* matrix specified by its set of Markov parameters specified by the underlying state-space model [24,31]

$$\mathcal{H}(t) = \underbrace{CA^{t-1}B + D}_{\text{Markov Parameters}}\ \delta(t) \tag{9}$$

B. Deconvolution

The basic deterministic multichannel deconvolution problem can be defined mathematically as:

GIVEN an N_y-vector measurement sequence $\{\mathbf{y}(t)\}; t = 1, \cdots, N_t$ for $\mathbf{y} \in \mathcal{R}^{N_y \times 1}$, FIND the corresponding N_u-vector excitation (input) sequence, $\{\mathcal{U}(t)\}$

The direct solution to the deterministic deconvolution problem is given by

$$\underbrace{\mathcal{U}(t)}_{\text{Excitation}} = \underbrace{\mathcal{H}^{-1}(t)}_{\text{Inverse Impulse Response}} \star \underbrace{\mathbf{y}(t)}_{\text{Measurement}} \tag{10}$$

or in the $\mathcal{Z}$-domain as

$$\underbrace{\mathcal{U}(z)}_{\text{Excitation}} = \underbrace{\mathcal{H}^{-1}(z)}_{\text{Inverse Transfer Function}} \times \underbrace{\mathbf{Y}(z)}_{\text{Measurement}} \tag{11}$$

Therefore, it is clear mathematically why this problem is termed an "inverse" problem—primarily because the system impulse response or transfer function matrices must be inverted in order to recover the excitation signal. Approaches to solve the deconvolution problem range from a simple division of Fourier spectra to more sophisticated Wiener inversions using smoothed power spectra to achieve reasonable results for the single channel case.[24] However, all attempts in the multichannel case usually result in transfer function modeling approaches and time domain solutions as in the seismic case.[2] For multichannel acoustic systems, a state-space model is one of the fundamental mechanisms applicable.[10,25,27]

The multiple channel models can be developed, starting with a set of input/output representations eventually leading to a set of *deterministic* state-space models. Typical *discrete-time* deterministic multiple input/multiple output (*MIMO*) systems can be characterized by their impulse response matrices or equivalently multichannel transfer function matrices. The impulse response of a discrete-time system is

$$\mathbf{y}(t) = \mathcal{H}(t) \star \mathbf{u}(t) = \sum_{k=0}^{K} \mathcal{H}(t-k)\mathbf{u}(k) \tag{12}$$

with t is the discrete-time index, $\star$ the multichannel *convolution* operator and $\mathbf{y} \in \mathrm{R}^{N_y \times 1}$, the vector of outputs, $\mathbf{u} \in \mathrm{R}^{N_u \times 1}$, the vector of inputs, $\mathcal{H} \in \mathrm{R}^{N_y \times N_u}$ the *impulse response matrix* with corresponding *transfer function matrix*, $\mathcal{H}(z) \in \mathcal{C}^{N_y \times N_u}$.

The impulse response can be represented as a multichannel matrix in terms of its inputs (columns) and outputs (rows) or equivalently in terms of column vector functions ($\mathbf{h}_i(t) \in$

$\mathcal{R}^{N_y} \times 1$) or row vector functions ($\mathbf{h}_i^T(t) \in \mathcal{R}^{N_u} \times 1$), that is,

$$\mathcal{H}(t) = \text{Outputs} \left\{ \underbrace{\begin{bmatrix} h_{11}(t) & \cdots & h_{1N_u}(t) \\ \vdots & \ddots & \vdots \\ h_{N_y1}(t) & \cdots & h_{N_yN_u}(t) \end{bmatrix}}_{\text{Inputs}} \right\} = [\mathbf{h}_1(t) \mid \cdots \mid \mathbf{h}_{N_u}(t)] = \begin{bmatrix} \mathbf{h}_1^T(t) \\ --- \\ \vdots \\ --- \\ \mathbf{h}_{N_y}^T(t) \end{bmatrix} \quad (13)$$

The multichannel convolution operations are then defined in terms of this representation as:

$$\mathbf{y}(t) = \mathcal{H}(t) \star \mathbf{u}(t) = [\mathbf{h}_1(t) \mid \cdots \mid \mathbf{h}_{N_u}(t)] \star \mathbf{u}(t) = [\mathbf{h}_1(t) \star \mathbf{u}(t) \mid \cdots \mid \mathbf{h}_{N_u}(t) \star \mathbf{u}(t)] \quad (14)$$

and therefore,

$$\begin{aligned} \mathbf{y}(t) = \mathcal{H}(t) \star \mathbf{u}(t) &= \begin{bmatrix} h_{11}(t) \star u_1(t) & \cdots & h_{1N_u}(t) \star u_{N_u}(t) \\ \vdots & \ddots & \vdots \\ h_{N_y1}(t) \star u_1(t) & \cdots & h_{N_yN_u}(t) u_{N_u}(t) \end{bmatrix} \\ &= \begin{bmatrix} \sum_{k=0}^{K} h_{11}(k) u_1(t-k) & \cdots & \sum_{k=0}^{K} h_{1N_u}(k) u_{N_u}(t-k) \\ \vdots & \ddots & \vdots \\ \sum_{k=0}^{K} h_{N_y1}(k) u_1(t-k) & \cdots & \sum_{k=0}^{K} h_{N_yN_u}(k) u_{N_u}(t-k) \end{bmatrix} \end{aligned} \quad (15)$$

where $h_{mn}(t)$ the impulse response from the n-th input excitation ($u_n(t)$) measured at the m-th output channel ($y_m(t)$); for $m = 1, \cdots, N_y$; and $n = 1, \cdots, N_u$.

The multichannel transfer function matrix follows by applying the $\mathcal{Z}$-transform to obtain

$$\mathcal{H}(z) = \begin{bmatrix} H_{11}(z) & \cdots & H_{1N_u}(z) \\ \vdots & \ddots & \vdots \\ H_{N_y1}(z) & \cdots & H_{N_yN_u}(z) \end{bmatrix} = [\mathbf{H}_1(z) \cdots \mathbf{H}_{N_u}(z)] \qquad \text{for} \qquad \mathbf{H}_n \in \mathcal{C}^{N_y \times 1} \quad (16)$$

The multichannel system can also be represented in state-space form with the impulse response matrix given in terms of its Markov parameters

$$\mathcal{H}(t) = \underbrace{CA^{t-1}B + D\delta(t)}_{\text{Markov Parameters}}; \quad t = 0, 1, \cdots, N \tag{17}$$

such that

$$\mathcal{H}(t) = \begin{bmatrix} \mathbf{c}_1^T A^{t-1}\mathbf{b}_1 + d_{11}\delta(t) & \cdots & \mathbf{c}_1^T A^{t-1}\mathbf{b}_{N_u} + d_{1N_u}\delta(t) \\ \vdots & \ddots & \vdots \\ \mathbf{c}_{N_y} A^{t-1}\mathbf{b}_1 + d_{N_y1}\delta(t) & \cdots & \mathbf{c}_{N_y}^T A^{t-1}\mathbf{b}_{N_u} + d_{N_yN_u}\delta(t) \end{bmatrix} \tag{18}$$

with the corresponding transfer function matrix in state-space form given by

$$\mathcal{H}(z) = \begin{bmatrix} \mathbf{c}_1^T (zI - A)^{-1}\mathbf{b}_1 + d_{11} & \cdots & \mathbf{c}_1^T (zI - A)^{-1}\mathbf{b}_{N_u} + d_{1N_u} \\ \vdots & \ddots & \vdots \\ \mathbf{c}_{N_y}^T (zI - A)^{-1}\mathbf{b}_1 + d_{N_y1} & \cdots & \mathbf{c}_{N_y}^T (zI - A)^{-1}\mathbf{b}_{N_u} + d_{N_yN_u} \end{bmatrix} \tag{19}$$

demonstrating the fact that the input/state/output representation captures the input/output as well as the internal structure of the underlying system in terms of its state variables and equivalent impulse response/transfer function matrices.

C. Gauss-Markov and Innovation Models

Incorporating noise and uncertainty into the basic multichannel problem, the *stochastic* deconvolution problem evolves.[6,24,25] Applying more structure to this stochastic problem leads to a linear, time-invariant *Gauss-Markov model* (*GM*) with *correlated noise sources* (see Fig. 1(a)) for stationary processes as:

$$\begin{aligned} \mathbf{x}(t+1) &= A\mathbf{x}(t) + B\mathbf{u}(t) + \mathbf{w}(t) \\ \mathbf{y}(t) &= C\mathbf{x}(t) + D\mathbf{u}(t) + \mathbf{v}(t) \end{aligned} \tag{20}$$

where $\mathbf{x},\mathbf{w} \in \mathcal{R}^{N_x \times 1}$, $\mathbf{y},\mathbf{v} \in \mathcal{R}^{N_y \times 1}$ and $\mathbf{u} \in \mathcal{R}^{N_u \times 1}$ with $A \in \mathcal{R}^{N_x \times N_x}$, $B \in \mathcal{R}^{N_x \times N_u}$, $C \in \mathcal{R}^{N_y \times N_x}$, $D \in \mathcal{R}^{N_y \times N_u}$, $\mathbf{w} \sim \mathcal{N}(0, R_{ww})$, $\mathbf{v} \sim \mathcal{N}(0, R_{vv})$ and the cross-covariance matrix given by $\text{cov}(\mathbf{w}, \mathbf{v}) = R_{wv}$. (Here the notation $\mathcal{N}(\mu, \mathbf{V})$ defines a Gaussian distribution of mean vector μ and variance matrix $\mathbf{V}$).

Noisy data must be processed to increase the signal-to-noise ratio (*SNR*) enabling the recovery problem to succeed. A state-space processor based on the Gauss-Markov representation leads directly to an optimal solution—the Kalman filter. It produces enhanced estimates of both the states and measurements while providing the all important innovations (residual error) sequence for performance analysis.[24,27] The basic state estimation problem is to find the minimum variance estimate of the state vector of the *GM*-model in terms of the currently available measurement sequence $y(t)$.

The innovations (*INV*) representation of the Kalman filter in "prediction form" is given by (see Refer. 27 for details)

$$\begin{aligned} \hat{\mathbf{x}}(t+1) &= A\hat{\mathbf{x}}(t) + B\mathbf{u}(t) + K_p(t)\mathbf{e}(t) && \text{[State Estimate]} \\ \mathbf{e}(t) &= \mathbf{y}(t) - \underbrace{C\hat{\mathbf{x}}(t)}_{\hat{\mathbf{y}}(t)} && \text{[Innovation]} \end{aligned} \tag{21}$$

with $\mathbf{e}(t)$ the *innovations sequence*, $\hat{\mathbf{y}}(t)$ the *estimated measurement* and $K_p(t)$ the *predicted Kalman gain* for correlated noise sources R_{wv} with state error covariance $\tilde{P}(t)$ given by

$$\begin{aligned} R_{ee}(t) &= C\tilde{P}(t)C' + R_{vv}(t) && \text{[Innovations Covariance]} \\ K_p(t) &= \Big(A\tilde{P}(t)C' + R_{wv}(t)\Big)R_{ee}^{-1}(t) && \text{[Kalman Gain]} \\ \tilde{P}(t+1) &= A\tilde{P}(t)A' - K_p(t)R_{ee}(t)K_p'(t) + R_{ww}(t) && \text{[Error Covariance]} \end{aligned} \tag{22}$$

where the *innovations model* can be defined in terms of the Kalman filter parameters as $\Sigma_{INV} := \{A, C, \tilde{P}, K_p, R_{ee}\}$.

With this information in mind, the solution to the multichannel deconvolution problem is based on designing and applying an inverse filter to recover the excitation as shown in Eq. 11. A direct model of an inverse filter is quite difficult to obtain analytically; however, we apply a subspace identification technique (*N4SID*) to solve the multichannel deconvolution problem.[28] Essentially, this approach is used to design a "shaping filter" (see Ref. 24) based on the state-space approach using representative excitation signals and apply it directly noisy

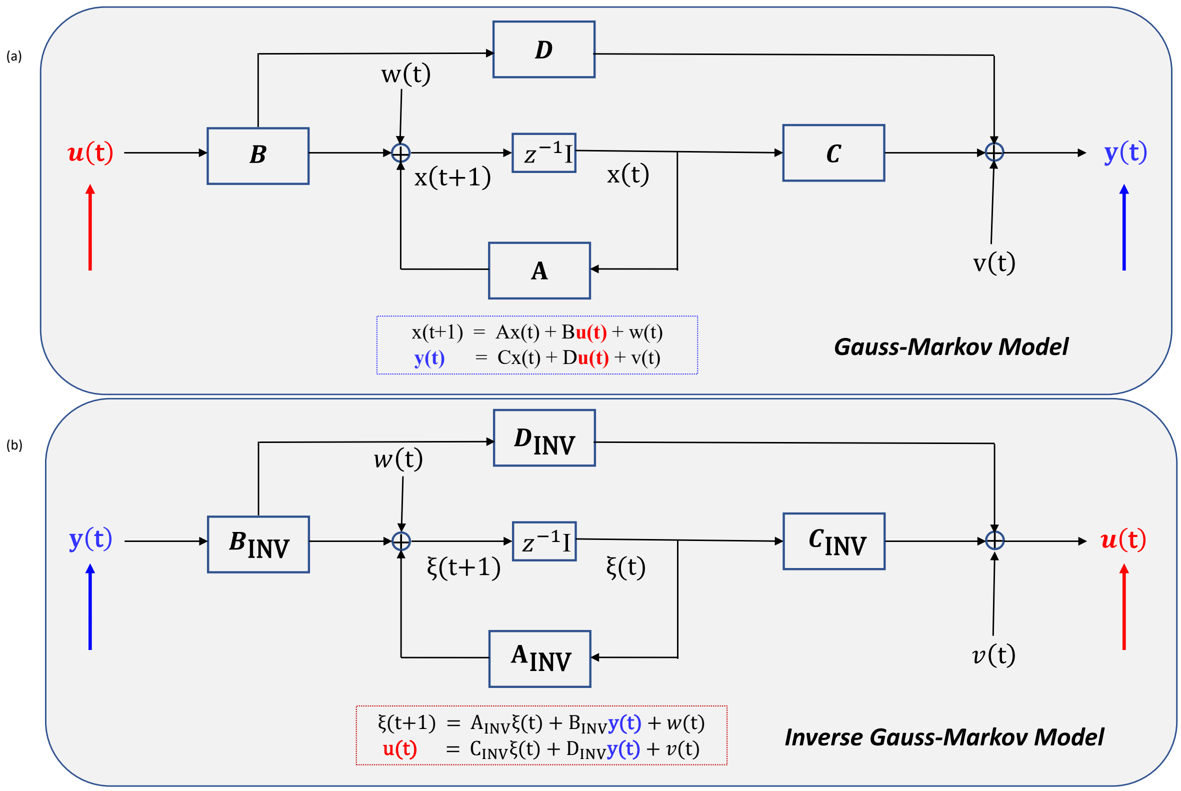

Figure 1: State-Space Realizations of Gauss-Markov and Inverse Filters: (a) Gauss-Markov model: Input: ($\mathbf{u}(t)$) and Output: ($\mathbf{y}(t)$). (b) Inverse Gauss-Markov (shaping) filter: Input: ($\mathbf{y}(t)$) and Output: ($\mathbf{u}(t)$).

data. Once designed, the filter is applied to measured data extracting the desired excitation directly.

D. Inverse (Shaping) Filter

A shaping filter is developed directly from Wiener filtering theory where a filtered output (e.g. a pulse) is termed the "desired" signal (d) with the measured data (y) as input. The objective is to develop a filter response capable of producing the desired signal or *shaping* the output, that is,

$$d(t) = \hat{\mathcal{F}}(t) \star y(t) \longrightarrow \hat{\mathcal{F}} = R_{yy}^{-1} R_{dy}$$

with covariance matrix/vector, R_{yy} and R_{dy}.[24]

For deconvolution, the shaping (inverse) filter is primarily developed to apply a set of calibration measurement data as *input* and produce the estimated excitations as *outputs*, that is, the filter is designed to create a processor that estimates the input excitations. First, the impulse response of the shaping filter or equivalently the multichannel state-space processor must be estimated during the *design* phase and next it must be *applied* to measured data as its input—the usual filtering operation. From the deconvolution problem perspective, the shaping filter is the required "inverse filter".

In the state-space framework, we have that $\Sigma_{inv} = \{A_{inv}, B_{inv}, C_{inv}, D_{inv}\}$ is characterized by

$$\begin{aligned} \xi(t+1) &= A_{inv}\xi(t) + B_{inv}\mathbf{y}(t) + w(t) && \text{[State]} \\ \mathbf{u}(t) &= C_{inv}\xi(t) + D_{inv}\mathbf{y}(t) + v(t) && \text{[Excitation]} \end{aligned} \tag{23}$$

where $\mathbf{y}$ is the new *input* and $\mathbf{u}$ is the new *output* of this inverse filter "shaping" it to be the actual excitation as shown in Fig. 1(b).

In summary, the multichannel shaping (inverse) filter *design* procedure is:

- *Obtain* excitation and multichannel sensor *calibration* data;
- *Design* inverse (shaping) filter, $\hat{\Sigma}_{inv} = \{\hat{A}_{inv}, \hat{B}_{inv}, \hat{C}_{inv}, \hat{D}_{inv}\}$, from calibration data using subspace identification (*N4SID*) techniques; and
- *Filter* subsequent measured data with the inverse filter to *extract* the excitations performing the deconvolution.

III. MULTICHANNEL DECONVOLUTION

The multichannel deconvolution processor was designed and applied to two sets of acoustic vibration data: (1) Transport Data; (2) Calibration Data. The transportation data was gathered using a tractor/trailer vehicle and a large mass to estimate typical roadway vibrations and shock events during shipping/handling operations. A test object response was investigated during a calibration experiment using a large shaker with random excitations. Both tests were employed to evaluate the feasibility of the inverse filter approach. Other simulations and data were also used and reported.[5,31,32]

A. Mass Transportation Experiment

A variety of excitations can occur during shipping and handling for transport any time during this process characterized by three typical excitations:[5,32]

- *DROP*—a drop can occur anytime during shipping/handling when the structural object is being placed in a container or trailer.
- *HAZARD*—a hazard can occur anytime during transit, once the object is placed in the transporter (truck, train, plane, ship, etc.).
- *ROAD*—a road induced vibration can occur anytime during transit on a roadway or rail or at sea/air.

The DROP is the most severe of excitations that can be directly applied to the structural object being transported. It can occur in a variety of situations when the object is being handled for shipping such as: forklift placement or moving the object through a variety of transporters (e.g. truck-to-train or truck-to-plane). The HAZARD excitation can also occur in a variety of manners. For instance, if construction were being performed on a road or railway with uneven surfaces being exposed as well as pot-holes on a road for example. The ROAD excitation induces a persistent vibrational response of the transported structural object during transit. Data were gathered, analyzed and used to synthesize potential responses evaluating the ability of the processor to extract these excitations employing an inverse multichannel filter—all of the results were successful as discussed in Ref. 32.

Mass transport experiments were performed by incorporating a 1500-lb concrete block mounted on a wooden shipping palate—the "Mass Transport Simulator".[5] The block synthesized a mock test object in size and shape and was transported in a 48-ft tractor/trailer over a typical transportation path in order to acquire shock and vibration data. The mass was mounted over the front axles and instrumented with tri-axial accelerometers located:

adjacent to the center-of-gravity of the block, centered in the trailer bed and above the rear axle as illustrated in Fig.2.

Data were acquired at a $10KHz$ sampling frequency triggered by shock events during the transport. The raw data were filtered and decimated to a Nyquist frequency of $5KHz$. This data set contains a *high* g-shock event as recorded over the rear axle on channels $4-6$. The shock, a HAZARD, was produced (unintentionally) by the tractor/trailer riding over a large road surface separation at different levels causing a g-force event as shown by the large transient recorded on the Z-direction channel (No. 6) and indicated on the X, Y-channels (No. 4 and 5) as well.

The processing approach is shown in Fig. 2 where the multichannel measurements are band-pass filtered using a 10^{th}-order Butterworth filter between the frequency band of $60Hz$ to $4.5KHz$ based on the range of expected rigid body modes of the vibrating structure ($< 60Hz$). The data were equalized (pre-whitened) to ensure a wide bandwidth for deconvolution. Once these data were available, the "average" impulse response along with the upper accelerometer measurements were used in an optimal deconvolution (single channel) scheme to extract the shock excitation for analysis. The resulting signal was investigated further applying a spectrogram processor to generate a frequency-time evolution analysis of the vibrational response as well as the deconvolution processor as illustrated.

The excitation and accelerometer data were pre-processed (filtered, decimated, trend removed, normalized) as shown in Fig. 3(a) where a set of extracted shock excitation transients and their corresponding ensemble spectra are given along with the subsequent response data and spectra in (b). Multichannel deconvolution (design) was performed by estimating (N4SID) an inverse filter using a 40-th order state-space model applying the excitation data as the *output* and the response data as the *input*.[20,28,29]

The results of the inverse filter design are shown in Fig. 4 where the true excitation data (turquoise) and their estimates (red) are overlayed in (a). Recall that the Z-M test requires that the estimate should lie below the bound (0.17) , while the W-T insists that 95% of each channel correlation estimates lie within the bounds or equivalently 5% are outside. For the design, the Z-M/W-T results for each measurement are: (No. 1: 0.022/6.3%), (No. 2: 0.058/6.3%), (No. 3: 0.026/4.7%). The application of the inverse filter processor to measurement data is shown in Fig. 5 where the average data spectrum is compared to the

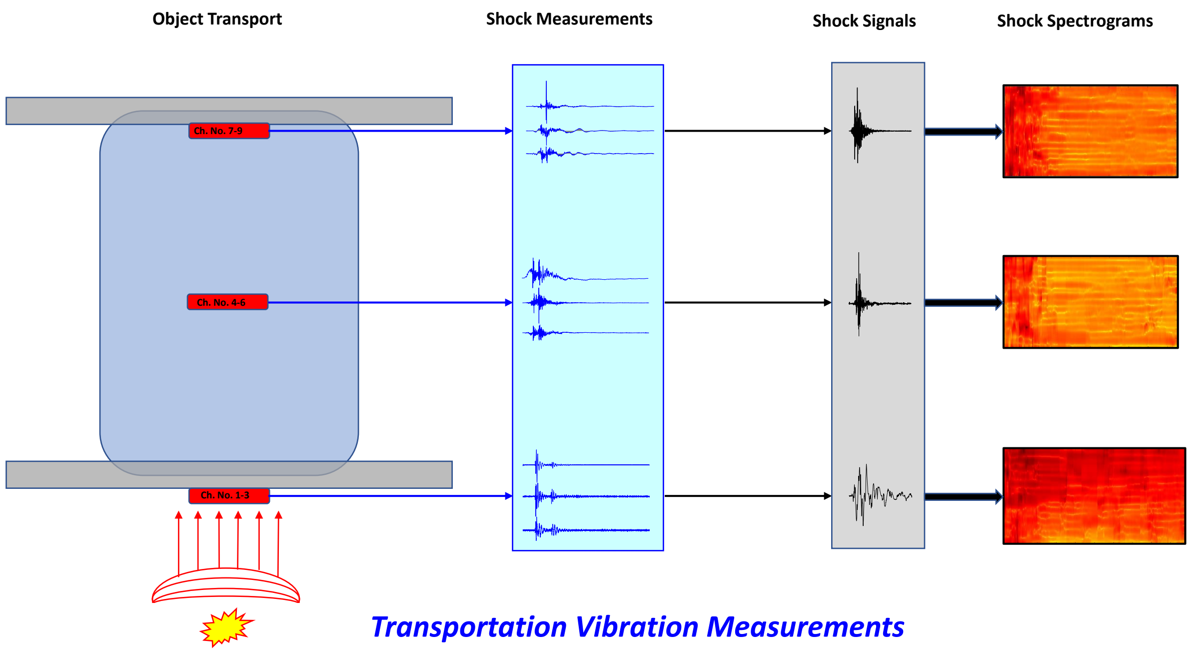

Figure 2: Transportation Vibration Measurements and Processing for Analysis: Test object transport structure with shock excitation, multichannel accelerometer measurements, processed signals and analysis spectrogram.

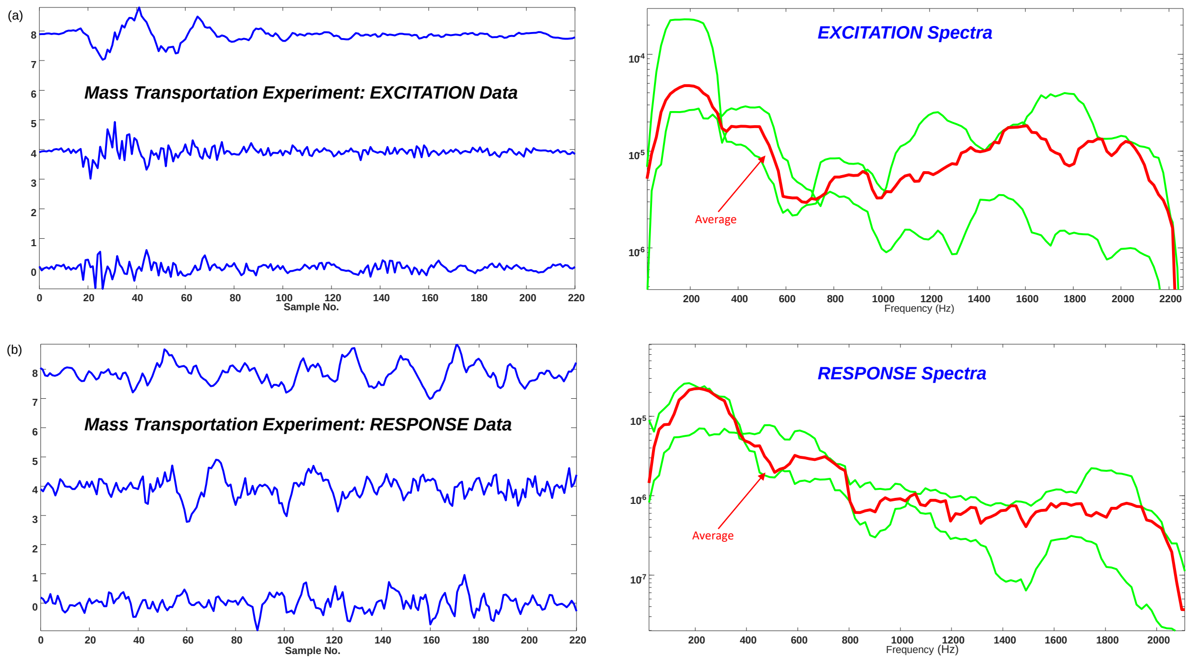

Figure 3: Mass Transportation Experiment Data: (a) Multichannel excitation (input) data and ensemble (thin line) with average (thick line) spectra. (b) Multichannel response (output) data and ensemble (thin line) with average (thick line) spectra.

average deconvolved spectrum. The results are encouraging, since the spectral bands of high interest are captured by the processor.

B. Test Object Calibration Experiment

Calibration tests are usually performed before shipping any acoustical object to ensure its proper operation especially for delicate instruments. The application of the multichannel deconvolution approach to an "unknown" structural test object is the focus of this effort. These tests are performed on this object that is essentially a complex, stationary structure with no rotating parts that is subjected to random excitations with accelerometers placed on its surface and around its periphery. Here the primary objective is to examine the feasibility of applying the model-based deconvolution technique to a mulitple input/multiple (*MIMO*) structural object with minimal a priori information subjected to environmental disturbances and noise.

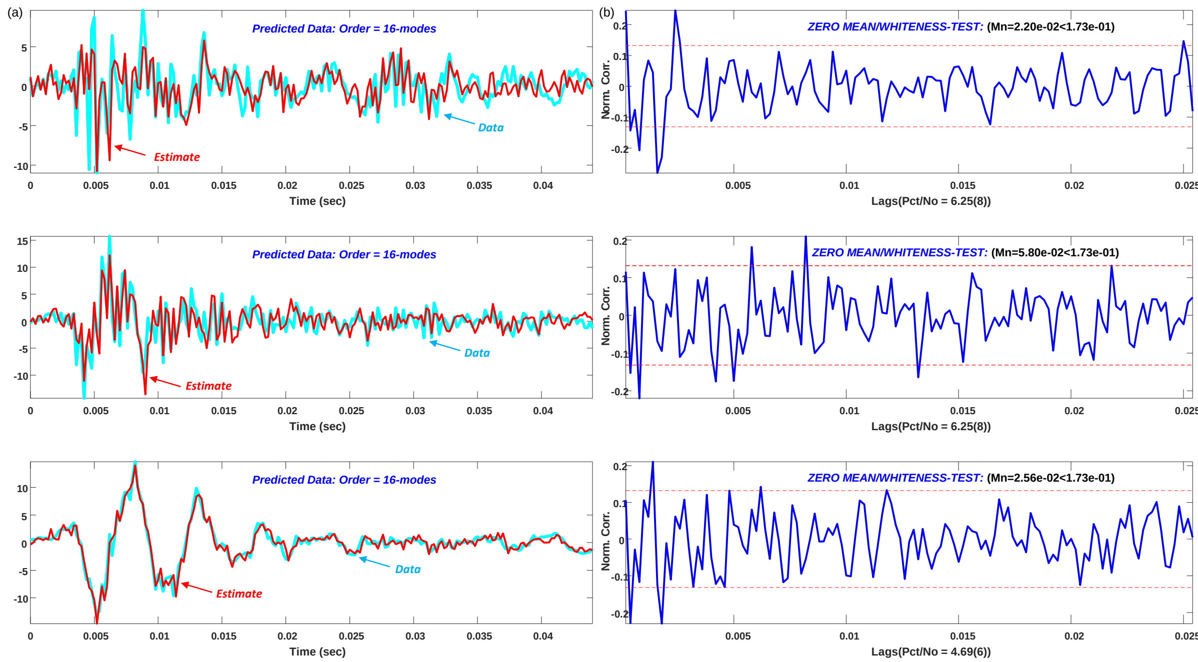

Figure 4: Mass Transportation Experiment: Inverse Filter Design for Excitation Recovery (Deconvolution). (a) *Design:* Recovery (multichannel) subspace (order = 16-modes) estimates with true-mean outputs. (b) *Performance:* Zero-Mean/Whiteness optimality tests: Z-M/W-T are: (No. 1: 0.022/6.3%), (No. 2: 0.058/6.3%), (No. 3: 0.026/4.7%).

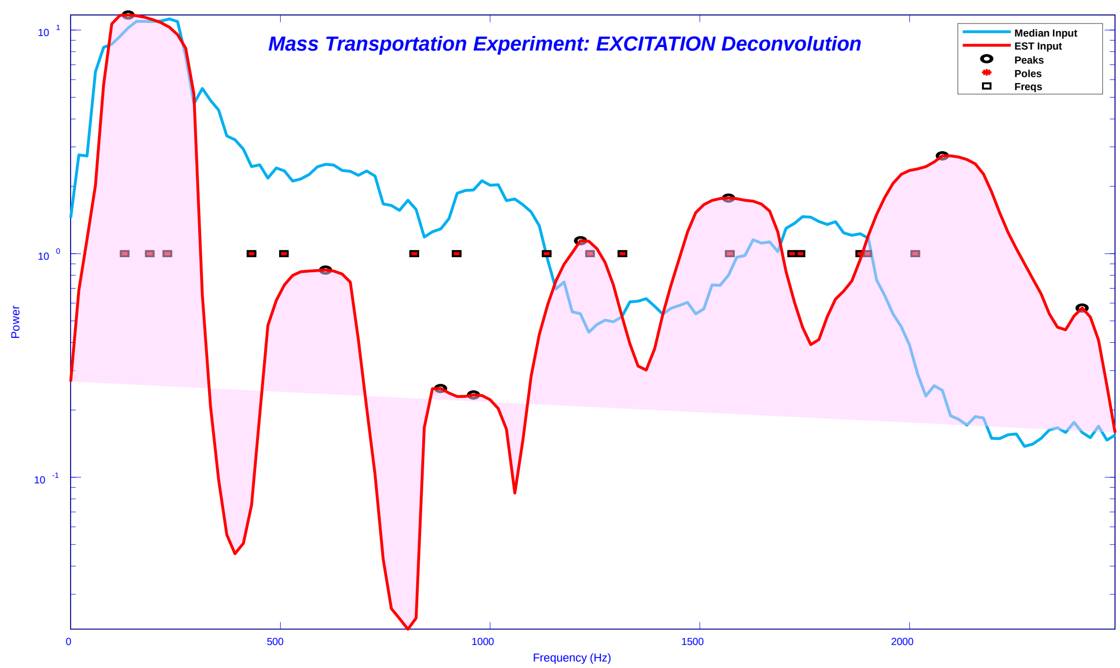

Figure 5: Mass Transportation Experiment Inverse Filter Design Spectra: Median excitation spectrum and average recovered (deconvolved) excitation (filled) spectral estimate.

The object under test is subjected to random excitations by placing a stinger or motor-driven rod perpendicular to the base of the structure as illustrated in Fig. 6. A suite of 19-triaxial (XYZ) accelerometers is positioned strategically about the surface of the structural object along with a single triaxial sensor allocated to measure the stinger xcitation time series. In total, an array of 57-accelerometer channels acquired a set of 10-minute duration data at a $6.4KHz$ sampling frequency.[24,31] For pre-processing the data were subsequently down-sampled to $2.5KHz$ in order to focus on the range of the excitation frequencies $(< 1.25KHz)$. For this investigation, a subset of 8-triaxial accelerometers is selected as well as the single triaxial sensor measuring the stinger excitation. Therefore, from the state-space perspective our *MIMO*-system, is a targeted system of up to a maximum of 12-modes or 24-states with an array of 24-channels (XYZ) of time series measurements and 3-channels (XYZ) of an excitation measurement that we are attempting to recover from these noisy accelerometer measurements using an inverse filter.

The raw (down-sampled) data represent the expected data windows (5000 samples) acquired from a real-time acquisition system. The windowed responses (time series) were

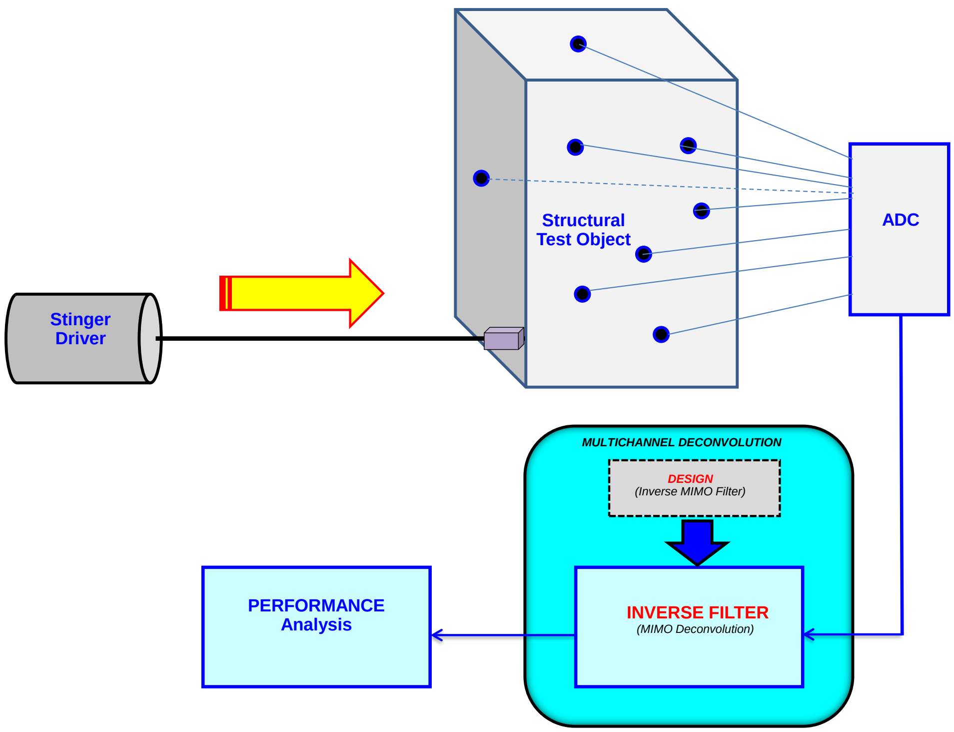

Figure 6: Structural Test Object Experimental Setup: Motor driven stinger (random excitations), accelerometer sensor measurements, *MIMO* analog-to-digital (A/D) acquisition, inverse filter (DESIGN), multichannel deconvolution,(INVERSE FILTERING), performance analysis.

pre-processed, that is, they were outlier corrected, equalized (whitening filter), bandpass filtered ($150 - 1.1KHz$), and normalized (mean removal/unit variance) prior to performing the inverse filter design. Once pre-processed the input/output data with roles reversed were provided to the subspace algorithm enabling an identification of a stability constrained, state-space model of the inverse filter, $\Sigma_{inv} = \{A_{inv}, B_{inv}, C_{inv}, D_{inv}\}$. Once the design accomplished, the inverse filter is applied to an independent section (5000 samples) of noisy accelerometer data to validate multichannel deconvolution processor performance.

The *MIMO*-data of the controlled experiment are shown in Fig. 7 where the triaxial (random) excitations with their accompanying ensemble spectra are shown along with the 8-triaxial accelerometer responses (24-channels) on the surface and periphery of the structural object. The ensemble spectra bounded at $1100Hz$ of both excitations and responses are also shown with the average spectrum (thick line) as well. The question to be answered is whether or not the multichannel deconvolution technique using an inverse filter is capable for extracting these excitations from the noisy accelerometer measurement data. We investigate this problem in two-phases: XYZ-data sets individually (8 directional outputs and 1-input) and the combined measurement array directly (24-outputs and 3-excitations). The simpler XYZ-data sets are investigated first followed by the combination or batch data.

The design procedure is to: (1) *Calibration*: design the *MIMO*-inverse filter using the state-space subspace identification method constrained for stable solutions only; (2) *Application*: process the incoming accelerometer measurements with Σ_{inv} to extract the excitations. The performance metrics that can be used are: the percentage of model fit (Fit %) to the data and its corresponding mean-squared error (*MSE*). This procedure is applied, starting with the individual XYZ-directional data sets with the results for the X-channel data is shown in Fig. 8(a) where the estimated excitation (thin dotted-line) is overlaid on the actual (initial) excitation (thick line). The subspace "fit" using a 25-mode model to the data (excitation) is at 44.4% and the *MSE* at 0.29. The optimality tests (zero-mean/white) indicate an optimal subspace design as Z-M/W-T: 0.009/4.9%. Note that since the excitations are random signals, then a reasonable comparison is the power spectra as shown in (c). It is clear that the design spectrum (filled) has captured the prominent spectral characteristics of the original excitation. The application of the inverse filter to another section of noisy measurement data (8-channels) also demonstrates the robustness of this approach, since the extracted excitation spectrum (green) also captures the salient features of the original excitation data (thick line). The resonant peaks (inset list) and the identified modal peaks (squares) are also shown overlaid on the spectral plots.

The multichannel deconvolution results for the Y-channel data shown in Fig. 9. Again the estimated excitation (dotted line) is overlaid on the actual (initial) excitation (thick line) where the subspace "fit" using a 25-mode model to the data is at 55.8% and the *MSE* 0.17—somewhat better than that of the X-channel. The optimality tests (zero-mean/white) indicate an optimal subspace design as Z-M/W-T: 0.006/4.7% with slightly better statistics as well.

Finally for the individual directional data, the multichannel deconvolution of the Z-channel data is depicted in Fig. 10 as above. The results are better than those of the previous individual channel data primarily because of a higher directional sensitivity (better *SNR*) to the induced vibrations. In this case, the the subspace "fit" again using a 25-mode model to the data is at 66.0% (best) and the smallest *MSE* of 0.11—somewhat better than that of the other channels. The optimality tests (zero-mean/white) indicate an optimal subspace design as Z-M/W-T: 0.003/6.6% (slightly larger %).

Next we consider the "batch" of all of the sensors combined as a *MIMO*-system of 3-excitations (inputs) and 24-responses (outputs) of Fig. 7. The inverse filter design results as a *MIMO*-system is shown in Fig. 11 where the overlaid fits and Z-M/W-T are shown. Here the subspace "fits" using a 20-mode model to the excitation data are at (35%,33%,31%) and the respective *MSE* at 1.25 not as good as the individual XYZ-channel results. The optimality tests (zero-mean/white) were also not quite as good for an optimal subspace design as Z-M/W-T: (0.005/7.6%; 0.003/8.3%; 0.005/7.7%). This could be because a lower *SNR* for the combination of batch channels as well as the fact that individual deconvolvers were design directly from each excitation separately. Next the inverse filter was applied directly to the 24-channel response data with the results shown in Fig. 12 depicting the deconvolution of each of the raw excitation channels (dotted lines). The similarity to the channel excitation spectra (solid lines) is quite good and clearly captures the major frequencies (list) available from the subspace identification.

This completes the discussion of the results of applying the *MIMO* deconvolution technique using the multichannel inverse filter subspace design as compared to the individual

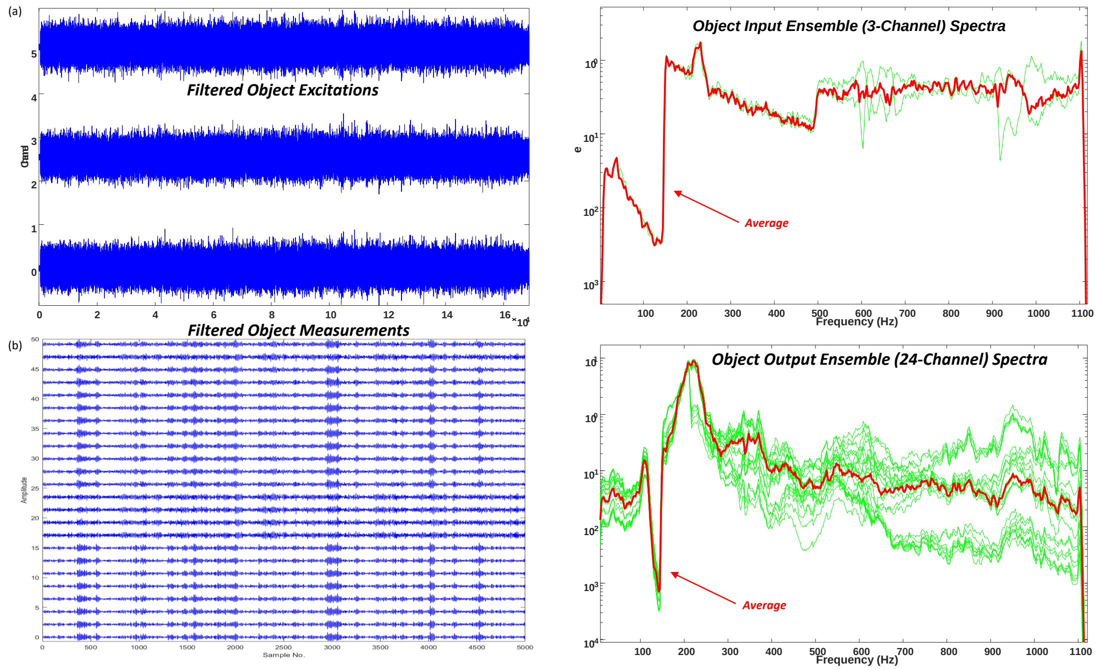

Figure 7: Test Object Data: (a) Multichannel (3-channels) random excitation (input) data and ensemble with average spectra. (b) Multichannel (24-channels) response (output) data and ensemble with average spectra.

channel designs. Even though the individual designs indicate a slightly superior performance, the batch design option may prove to be quite adequate in some applications. Thus, reasonable solutions to the multichannel deconvolution problem is successful on experimental data.

IV. SUMMARY

Transporting critical acoustical objects of high interest is a viable problem from the initial shipping/packaging and subsequent vibrational response inflicted during actual transport by rail, highway, sea or air. This leads to the need to extract any of the excitations incurred in order to assess the potential damage and assess potential structural failures. The multichannel deconvolution problem for transporting critical test objects is investigated by developing a shaping or inverse filter design based on a state-space (subspace) identification technique. The filter is designed during calibration tests and applied to noisy multichannel

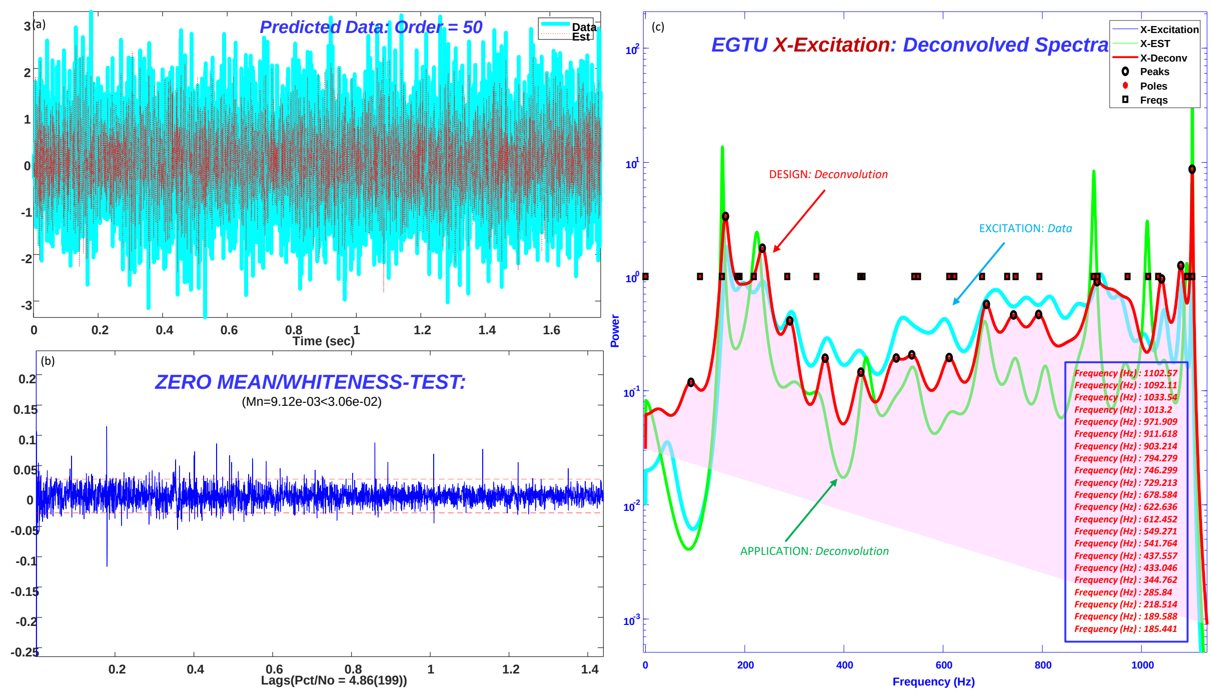

Figure 8: Test Object X-Channel Data (8-Measurements,1-Excitation): (a) *Design:* Recovery (multichannel) subspace estimates (Order = 25-modes, Fit = 44.4%, MSE = 0.29). (b) *Performance:* Zero-Mean/Whiteness optimality tests: Z-M/W-T are: (No. 1: 0.009/4.9%). (c) Deconvolution spectra: Excitation, inverse filtered application and design deconvolution with spectral peaks (circles) and eigen-frequencies (squares) including peak frequency estimates (list).

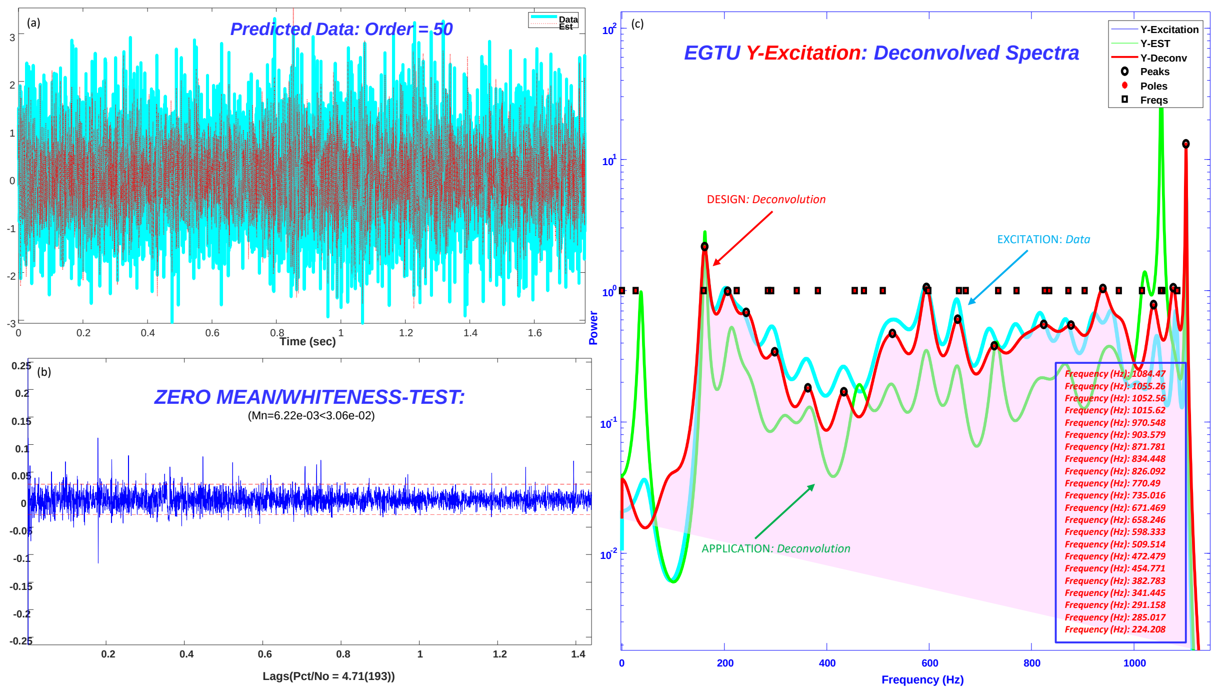

Figure 9: Test Object Y-Channel Data (8-Measurements,1-Excitation): (a) *Design:* Recovery (multichannel) subspace estimates (Order = 25-modes, Fit = 55.8%, MSE = 0.17). (b) *Performance:* Zero-Mean/Whiteness optimality tests: Z-M/W-T are: (No. 1: 0.006/4.7%). (c) Deconvolution spectra: Excitation, inverse filtered application and design deconvolution with spectral peaks (circles) and eigen-frequencies (squares) including peak frequency estimates (list).

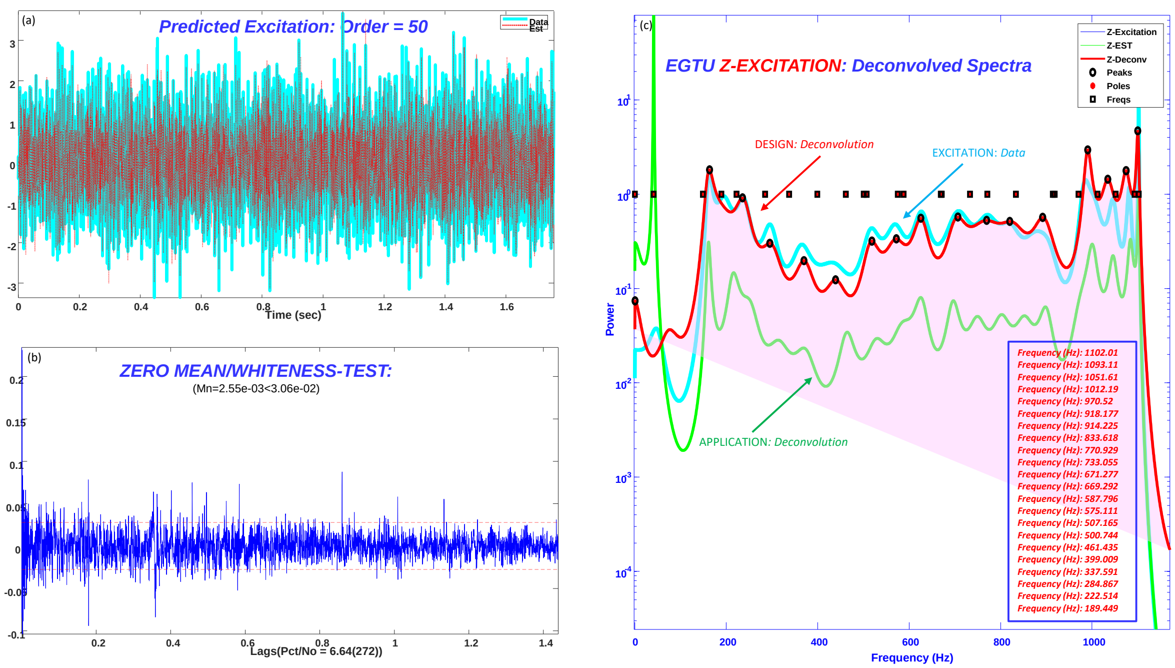

Figure 10: Test Object Z-Channel Data (8-Measurements,1-Excitation): (a) *Design:* Recovery (multichannel) subspace estimates (Order = 25-modes, Fit = 66.0%, MSE = 0.11). (b) *Performance:* Zero-Mean/Whiteness optimality tests: Z-M/W-T are: (No. 1: 0.003/6.6%). (c) Deconvolution spectra: Excitation, inverse filtered application and design deconvolution with spectral peaks (circles) and eigen-frequencies (squares) including peak frequency estimates (list).

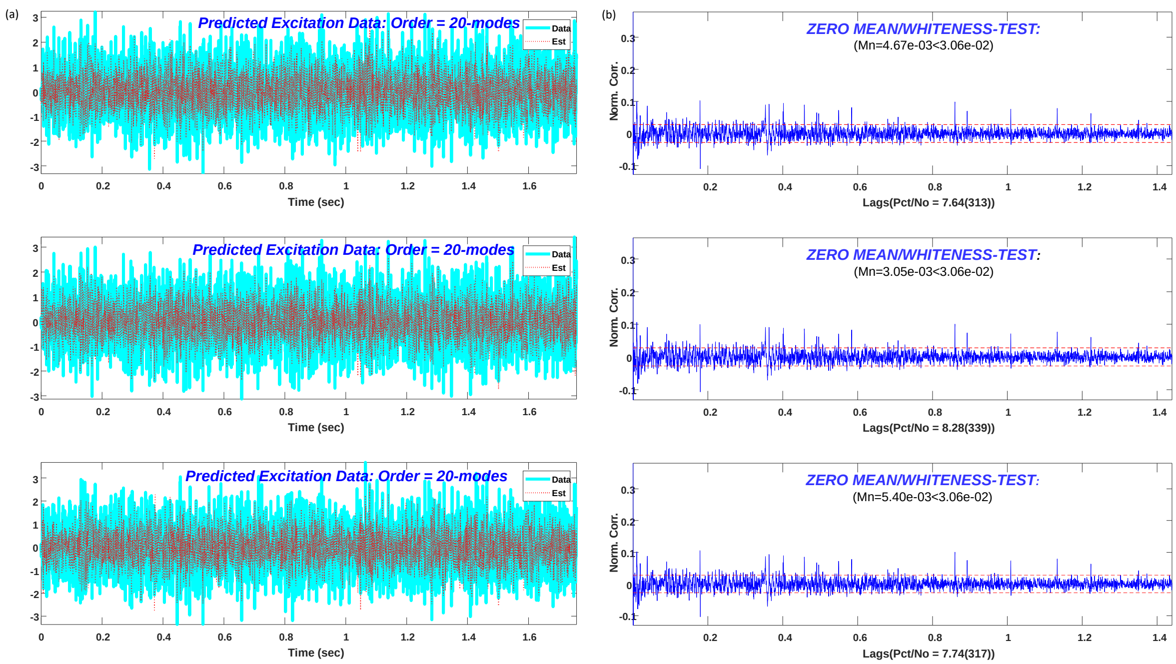

Figure 11: Test Object DESIGN: Inverse Filter Design (3-Channels) for Excitation Recovery (Deconvolution). (a) *Design:* Recovery (multichannel) subspace (Order = 20-modes, Fits = 35%,33%,31%) estimates with corresponding raw excitation data to match and *Performance:* Zero-Mean/Whiteness optimality tests: Z-M/W-T are: (No. 1: 0.005/7.6%), (No. 2: 0.003/8.3%), (No. 3: 0.005/7.7%).

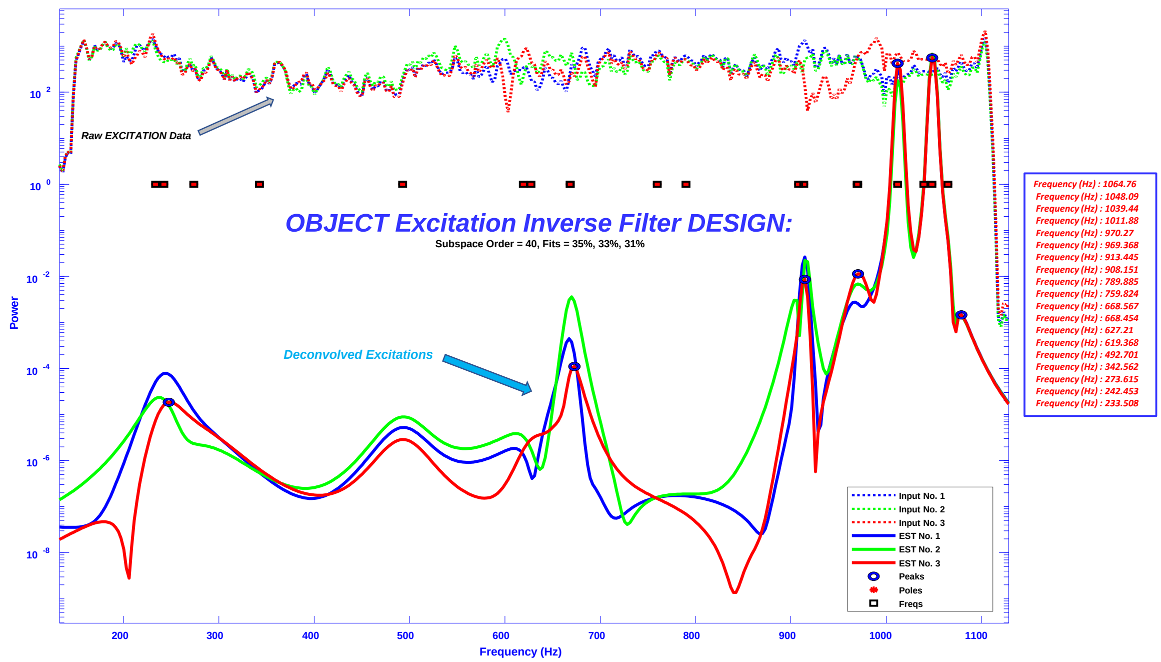

Figure 12: Test Object Inverse Filter Design Spectra: Raw excitation (dotted lines) spectra (3-Channels) and recovered (deconvolved) excitation (solid lines) spectral estimates with spectral peaks (circles) and eigen-frequencies (squares) including peak frequency estimates (list).

accelerometer measurement data demonstrating a reliable and timely approach to solving this critical problem.

A *Mass Transportation Experiment* is performed employing a large concrete block as a test object that was packaged and shipped in an instrumented tractor/trailer vehicle along typical roadways to obtain both excitation and response signals for analysis and performance evaluations. The basic idea is to extract shock and vibration excitation signals that test objects experience during a typical transport scenario. During this transport "known" shocks (drops) occur and are processed along with minor shocks during various segments of travel yielding valuable data sets. The results of applying a model-based deconvolution are quite reasonable enabling a successful extraction of the excitation inputs.

Finally, the vibrational response of a structural test object is investigated during a calibration test with recorded random excitation inputs from a shaker. Again the results are quite encouraging indicating that the shaping or inverse filter design and application provide a meaningful methodology that can be applied to extract random transient excitations during transport of critical structural test objects to assess potential damage and ensure reliable operation.

II Acknowledgments

This work performed under the auspices of the U.S. Department of Energy by Lawrence Livermore National Laboratory under Contract DE-AC52-07NA27344. The authors would like to recognize Mr. H. Teng and Mr. S. Franco for providing the data sets for the mass transportation experiment and test object shaker data along with Mr. J. Case, B. Illingworth and J. Cook for helpful discussion on the problem throughout this effort.

APPENDIX A: Subspace Identification Method

In this appendix, we briefly summarize the major points of the **n**umerical algorithm **for** state space **s**ubspace system **id**entification (*N4SID*) technique.[28] Primarily, subspace techniques extract an extended observability matrix directly from the acquired data first, followed by estimating the state-space, system model (Σ_{ABCD}) (see Refr. 20, 28 − 30 for more details). The *observability matrix* to be extracted is defined by

$$\mathcal{O}_k := \begin{bmatrix} C \\ --- \\ \vdots \\ --- \\ CA^{k-1} \end{bmatrix} \tag{24}$$

The underlying mathematical foundation that enables these extractions is projection theory. The primary idea, when applied to this problem, is to perform projections in a Hilbert space occupied by random vectors. That is, if $\mathbf{y}_f(t)$ is a random vector (finite) of *future outputs* and $\mathbf{y}_p(t)$ a random vector of *past outputs*, then the projection of the "future output data onto the past output data" $\mathcal{P}_{y_f|y_p}$ is invoked by applying the *projection operator* onto the past output data space to the future output data.

This idea of projecting a vector onto a subspace spanned by another vector can be extended to projecting a row space of a matrix onto the row space of another matrix.[20,28−30] Invoking oblique projections of the row space of future data $\mathcal{Y}_f$ onto the row space of past data $\mathcal{Y}_p$ enables us to extract both the extended observability matrix as well as the estimated state vectors by applying a singular value decomposition (*SVD*) operation, that is,[20]

$$\mathcal{P}_{\mathcal{Y}_f|\mathcal{Y}_p} = \mathcal{O}_k \hat{\mathcal{X}}_k = \underbrace{\left(U_{N_x} \Sigma_{N_x}^{1/2}\right)}_{\mathcal{O}_{N_x}} \underbrace{\left((\Sigma'_{N_x})^{1/2} V'_{N_x}\right)}_{\hat{\mathcal{X}}_k} \tag{25}$$

where U_{N_x} and V'_{N_x} are the respective left and right orthogonal matrices of the *SVD* performed on a data matrix.[20]

This technique also requires a "shifted" projection $\mathcal{P}_{\mathcal{Y}_f^-|\mathcal{Y}_p^+}$ to extract the model. Here the operator projects shifted future data $\mathcal{Y}_f^-$ as a row and incorporates it into the past output data array such that $\mathcal{Y}_p \rightarrow \mathcal{Y}_p^+$. This projection, coupled with the first enables the extraction of estimated states, since it has been shown that[39]

$$\mathcal{P}_{\mathcal{Y}_f|\mathcal{Y}_p} \;=\; \mathcal{O}_k \times \hat{\mathcal{X}}_k \qquad \text{and} \qquad \mathcal{P}_{\mathcal{Y}_f^-|\mathcal{Y}_p^+} \;=\; \mathcal{O}_{k-1} \times \hat{\mathcal{X}}_{k+1} \qquad\qquad \text{[Projections]} \tag{26}$$

where $\mathcal{O}_{k-1}$ is the observability matrix with the last block row removed.

With this in mind, *both* states can be extracted directly from the projections using pseudo-inversion ($^{\#}$) to obtain

$$\hat{\mathcal{X}}_k \;=\; \mathcal{O}_k^{\#} \times \mathcal{P}_{\mathcal{Y}_f|\mathcal{Y}_p} = \mathcal{O}_k \times \hat{\mathcal{X}}_k \qquad \text{and} \qquad \hat{\mathcal{X}}_{k+1} \;=\; \mathcal{O}_{k-1}^{\#} \times \mathcal{P}_{\mathcal{Y}_f^-|\mathcal{Y}_p^+} = \mathcal{O}_{k-1} \times \hat{\mathcal{X}}_{k+1} \qquad \text{[States]} \tag{27}$$

With these states of a Kalman filter now available from the *SVD* and pseudo-inversions, the underlying "batch" state-space (innovations) model is

$$\begin{aligned} \hat{\mathcal{X}}_{k+1} &= A\,\hat{\mathcal{X}}_k \;+\; B\,\mathcal{U}_{k|k} + \xi_{\omega_k} \\ \hat{\mathcal{Y}}_{k|k} &= C\,\hat{\mathcal{X}}_k \;+\; D\,\mathcal{U}_{k|k} + \xi_{\nu_k} \end{aligned} \tag{28}$$

where the block data and input matrices are defined by $\mathcal{Y}_{k|k}$, $\mathcal{U}_{k|k}$, respectively and the corresponding system and measurement noise processes by $\xi_{\omega_k}, \xi_{\nu_k}$.[20,28]

The residuals or equivalently innovations sequence and its covariance are defined by

$$\xi := \begin{bmatrix} \xi_{\omega_k} \\ -- \\ \xi_{\nu_k} \end{bmatrix}; \quad \text{and} \quad R_{\xi\xi} := E\{\xi\xi'\} = E\left\{ \begin{bmatrix} \xi_{\omega_k} \\ -- \\ \xi_{\nu_k} \end{bmatrix} \begin{bmatrix} \xi_{\omega_k} & | & \xi_{\nu_k} \end{bmatrix}' \right\} \tag{29}$$

More compactly,

$$\underbrace{\begin{bmatrix} \hat{\mathcal{X}}_{k+1} \\ --- \\ \hat{\mathcal{Y}}_{k|k} \end{bmatrix}}_{\text{known}} = \begin{bmatrix} A & | & B \\ - & - & - \\ C & | & D \end{bmatrix} \underbrace{\begin{bmatrix} \hat{\mathcal{X}}_k \\ --- \\ \mathcal{U}_{k|k} \end{bmatrix}}_{\text{known}} + \begin{bmatrix} \xi_{\omega_k} \\ --- \\ \xi_{\nu_k} \end{bmatrix} \tag{30}$$

which can be solved as an estimation problem providing a *least-squares solution* as:

$$\begin{bmatrix} \hat{A} & | & \hat{B} \\ - & - & - \\ \hat{C} & | & \hat{D} \end{bmatrix} = \left(\begin{bmatrix} \hat{\mathcal{X}}_{k+1} \\ --- \\ \hat{\mathcal{Y}}_{k|k} \end{bmatrix} \begin{bmatrix} \hat{\mathcal{X}}_k \\ --- \\ \mathcal{U}_{k|k} \end{bmatrix}' \right) \left(\begin{bmatrix} \hat{\mathcal{X}}_k \\ --- \\ \mathcal{U}_{k|k} \end{bmatrix} \begin{bmatrix} \hat{\mathcal{X}}_k \\ --- \\ \mathcal{U}_{k|k} \end{bmatrix}' \right)^{-1} \tag{31}$$

with the corresponding "least-squares" residual (innovations) covariances estimated by

$$\hat{R}_{\xi\xi} = \begin{bmatrix} R^e_{\omega\omega} & | & R^e_{\omega\upsilon} \\ - & - & - \\ (R^e_{\omega\upsilon})' & | & R^e_{\upsilon\upsilon} \end{bmatrix} = \begin{bmatrix} KR_{ee}K' & | & KR^{1/2}_{ee} \\ - & - & - \\ (KR^{1/2}_{ee})' & | & R_{ee} \end{bmatrix} \tag{32}$$

leading to

$$\begin{aligned} \hat{R}_{ee} &\approx R^e_{\upsilon\upsilon} && \text{[Innovations Covariance]} \\ \hat{K} &\approx R^e_{\omega\upsilon}\hat{R}^{-1/2}_{ee} && \text{[Kalman Gain]} \end{aligned} \tag{33}$$

Thus, the solution of the stochastic realization problem, $\Sigma_{\text{INV}} = \{\hat{A}, \hat{B}, \hat{C}, \hat{D}, R^e_{\omega\omega}, R^e_{\omega\upsilon}, R^e_{\upsilon\upsilon}\}$, is obtained through solving these least-squares relations using the *N4SID*-method.[20,28]

[1] L. Sibul and M. Roan, "An overview of inverse problems in acoustic and seismic signal processing," J. Acoust. Society Amer., Vol. 115, pp 2470, 2004.

[2] E. Robinson and S. Treitel, Geophysical Signal Analysis (Prentice-Hall,New Jersey,1980).

[3] J. Cook, T. Coforth and R. Cook, "Seismic and underwater responses to sonic boom," J. Acoust. Society Amer., Vol. 49, pp 77, 1971.

[4] L. Dicus, "Impulse response estimation with underwater explosive charge acoustic signals," J. Acoust. Soc. Am. 70 (1), 122-133, 1981.

[5] S. Jensen and B. Markowicz, *Transportation Vibration Characterization of a 48' Air ride Trailer with 1500 lbs. Mass Load*, LLNL Internal Memo, 2016.

[6] J. Candy, K. Fisher, J. Case, B. Illingworth, K. Craft, "Excitation Recovery Problem: A Model-Based Approach to Multichannel Deconvolution", LLNL-Report, LLNL-TR-813769, 2020.

[7] P. Mignerey and S. Finette, "Multichannel deconvolution of an acoustic transient in an oceanic waveguide," J. Acoust. Society Amer., Vol. 92 (1), pp 351-364, 1992.

[8] T. Olofsson and T. Stepinski, "Maximum a posteriori deconvolution of ultrasonic signals using multiple transducers," J. Acoust. Soc. Am. 107 (6), 3276-3288, 2000.

[9] C-Y. Chi and W-T Chen, "An adaptive maximum-likelihood deconvolution algorithm," Signal Proc. 24, pp 149-163, 1991.

[10] J. Kormylo and J. Mendel, "Maximum-likelihood deconvolution", IEEE Trans. Geosci. Remote Sensing, Vol. GE-21, pp. 72-82, 1983.

[11] J. Candy, R. Ziolkowski, and K. Lewis, "Transient wave estimation: a multichannel deconvolution application," J. Acoust. Society Amer., Vol. 88 (5), pp 2235-2247, 1990.

[12] M. Tanter, J-L Thomas and M. Fink, "Time reversal and the inverse filter" J. Acoust. Soc. Am. 108 (1), 223-234, 2000.

[13] T. Gallot, S. Catheline, P. Roux and M. Campillo, "A passive inverse filter for Green's function retrieval" J. Acoust. Soc. Am. Exp. Letters, 131 (1), EL21-EL26, 2012.

[14] D. Beaton and N. Xiang,"Room acoustic modal analysis using Bayesian inference," J. Acoust. Soc. Am. 141(6), 4480-4493, 2017.

[15] E. Reynders, "System identification methods for (operational) modal analysis: review and comparison," *Archives of Comp. Methods Engr.*, Vol. 19 (1), pp. 51-124, 2012.

[16] L. Marple, *Digital Spectral Analysis*, 2nd-Ed., (Dover,NY,2019).

[17] E. Sullivan, *Model-Based Processing for Underwater Acoustic Arrays.* (Springer,NY,2015).

[18] J. Candy, K. Fisher, J. Case, and T. Goodrich, "Multichannel spectral estimation in acoustics: a state-space approach," J. Acoust. Soc. Am. 148(2), 759-779, 2020.

[19] B. Rao and K. Arun, "Model-based processing of signals: a state space approach." Proc. IEEE, Vol. 80, no. 2, pp. 283-309, 1992.

[20] J. Candy, *Model-Based Processing: An Applied Subspace Identification Approach.* (Wiley,Hoboken,NJ,2019).

[21] P. DeRusso, R. Roy, C. Close and A. Desroches, *State Variables for Engineers*, (Wiley,Hoboken,NJ,1998).

[22] R. Wiggins and E. Robinson,"Recursive solution to the multichannel filtering problem," J. Geophys. Res. 70(8), 1885-1891 (1965).

[23] J. Walsh, "On limitations of minimum mean-square error deconvolution in deriving impulse responses of rooms," J. Acoust. Soc. Am. 77 (2), pp 547-556, 1985.

[24] J. Candy, *Model-Based Signal Processing*, (Wiley,IEEE Press,Hoboken,NJ,2006).

[25] J. Mendel, *Maximum-likelihood Deconvolution: a Journey Into Model-based Signal Processing*, (Springer,NY,1990).

[26] A. Baggeroer, W. Kuperman, and H. Schmidt, "Matched-field processing: source localization in correlated noise as an optimum parameter estimation problem," *J. Acoust. Soc. Am*, **83**, (2), 571-587, 1988.

[27] J. Candy, J. Case, K. Fisher, B. Illingworth K. Craft, "Transient recovery problem in acoustics: a multichannel model-based deconvolution approach," *J. Acoust. Soc. Am.*, Vol. 143, (2), pp. 680-696, 2020.

[28] P. van Overschee and B. De Moor, "N4SID: Numerical algorithms for state space subspace system identification." Automatica, vol 30, pp. 75-93, 1994.

[29] P. van Overschee and B. De Moor, *Subspace Identification for Linear Systems: Theory, Implementation, Applications.* (Kluwer Academic,Boston,MA,1996).

[30] T. Katayama, *Subspace Methods for System Identification.* (Springer,London,UK,2005).

[31] J. Candy, S. Franco, E. Ruggiero, M. Emmons, I. Lopez and L. Stoops, "Anomaly detection for a vibrating structure: A subspace identification/tracking approach," *J. Acoust. Soc. Am.*, Vol. 142, (2), pp. 680-696, 2017.

[32] J. Candy, K. Fisher, B. Markowicz, D. Paulsen, "Multichannel Deconvolution of Vibrational Shock Signals: An Inverse Filtering Approach", LLNL-Report, LLNL-TR-8117068, 2020.

LIST OF FIGURES

covery (multichannel) subspace estimates (Order = 25-modes, Fit = 44.4%, MSE = 0.29). (b) *Performance:* Zero-Mean/Whiteness optimality tests: Z-M/W-T are: (No. 1: 0.009/4.9%). (c) Deconvolution spectra: Excitation, inverse filtered application and design deconvolution with spectral peaks (circles) and eigen-frequencies (squares) including peak frequency estimates (list).

FIG. 9 Test Object Y-Channel Data (8-Measurements,1-Excitation): (a) *Design:* Recovery (multichannel) subspace estimates (Order = 25-modes, Fit = 55.8%, MSE = 0.17). (b) *Performance:* Zero-Mean/Whiteness optimality tests: Z-M/W-T are: (No. 1: 0.006/4.7%). (c) Deconvolution spectra: Excitation, inverse filtered application and design deconvolution with spectral peaks (circles) and eigen-frequencies (squares) including peak frequency estimates (list).

FIG. 10 Test Object Z-Channel Data (8-Measurements,1-Excitation): (a) *Design:* Recovery (multichannel) subspace estimates (Order = 25-modes, Fit = 66.0%, MSE = 0.11). (b) *Performance:* Zero-Mean/Whiteness optimality tests: Z-M/W-T are: (No. 1: 0.003/6.6%). (c) Deconvolution spectra: Excitation, inverse filtered application and design deconvolution with spectral peaks (circles) and eigen-frequencies (squares) including peak frequency estimates (list).

FIG. 11 Test Object DESIGN: Inverse Filter Design (3-Channels) for Excitation Recovery (Deconvolution). (a) *Design:* Recovery (multichannel) subspace (Order = 20-modes, Fits = 35%,33%,31%) estimates (dotted lines) with corresponding raw excitation data to match (solid lines)) and *Performance:* Zero-Mean/Whiteness optimality tests: Z-M/W-T are: (No. 1: 0.005/7.6%), (No. 2: 0.003/8.3%), (No. 3: 0.005/7.7%).

FIG. 12 Test Object Inverse Filter Design Spectra: Raw excitation (dotted-lines) spectra (3-Channels) and recovered (deconvolved) excitation (solid lines) spectral estimates with spectral peaks (circles) and eigen-frequencies (squares) including peak frequency estimates (list).